

Improving entanglement and thermodynamic Rényi entropy measurements in quantum Monte Carlo

David J. Luitz, Xavier Plat, Nicolas Laflorencie, and Fabien Alet

Laboratoire de Physique Théorique, IRSAMC, Université de Toulouse, CNRS, 31062 Toulouse, France*

(Dated: May 30, 2014)

We present a method for improving measurements of the entanglement Rényi entropies in quantum Monte Carlo simulations by relating them with measurements of participation Rényi entropies. Exploiting the capability of building improved estimators for the latter allows to obtain very good estimates for entanglement Rényi entropies. When considering a full system instead of a bipartition, the method can be further ameliorated providing access to the thermodynamic Rényi entropies with high accuracy. We also explore a recently-proposed method for the reconstruction of the entanglement spectrum from entanglement Rényi entropies and finally show how potential entanglement Hamiltonians may be tested for their validity using a comparison with thermal Rényi entropies.

PACS numbers: 02.70.Ss, 03.67.Mn, 75.10.Jm, 05.10.Ln

I. INTRODUCTION

Quantum entanglement has been of interest since the early days of quantum mechanics¹. The quantification of the entanglement in interacting many body quantum systems has attracted a lot of attention during the last decade for several fundamental and practical reasons². Entanglement properties of one-dimensional quantum problems can be treated fully analytically only in a limited number of cases (see *e.g.* Refs. 3,4), or asymptotically for conformally invariant⁵ or some disordered systems⁶. They remain generically accessible to numerical Density Matrix Renormalization Group (DMRG) calculations, provided the entanglement between the subsystems is not too large⁷. For higher dimensional systems however, exact methods are much more difficult to implement. Nevertheless, remarkable progresses have been made recently, *e.g.* using series expansions^{8,9}, numerical linked cluster expansion^{10,11}, or using quantum Monte Carlo (QMC) simulations^{12–21}, which is precisely the topic of the present work.

In nonfrustrated quantum spin systems, standard thermodynamic observables can be obtained to very high accuracy within QMC simulations²². Here we are interested in the Rényi entanglement entropy (EE)

$$S_{A,q}^E = \frac{1}{1-q} \ln \rho_A^q, \quad (1)$$

where ρ_A is the reduced density matrix, assuming that A is a subsystem imbedded in a larger system. Clearly $S_{A,q}^E$ cannot be related to a simple thermodynamic observable, *e.g.* a correlation function (except for non-interacting systems^{23,24}). At zero temperature, Hastings *et al.*¹⁴ developed a technique based on the introduction of a “swap”-operator in a projector Monte Carlo approach to tackle this issue. At finite temperature, several techniques have been explored, including temperature integration¹⁵ and Wang Landau sampling²⁵.

Perhaps the most elegant method was brought forward by Humeniuk and Roscilde¹⁶. Their method for the calculation of entanglement Rényi entropies of order q for a

subsystem A in path integral QMC methods is based on the observation⁵ that they are related to the ratio of partition functions $\mathcal{Z}_{A,q}/\mathcal{Z}_{\emptyset,q}$. Here, $\mathcal{Z}_{A,q}$ is the partition function of q replicas glued together at one imaginary time slice on the subsystem A only. $\mathcal{Z}_{\emptyset,q} = \mathcal{Z}^q$ is the partition function of q independent replicas. Here and from now on, q is an integer ≥ 2 .

In a simulation which samples both partition functions in a generalized ensemble, proposing moves between the two ensembles, the estimator for the entanglement Rényi entropy is given by¹⁶:

$$\langle S_q^E \rangle_{MC} = \frac{1}{1-q} \ln \langle \frac{N_A}{N_{\emptyset}} \rangle_{MC}, \quad (2)$$

where N_A is the number of QMC configurations observed in the glued ensemble, while N_{\emptyset} is the number of QMC configurations seen in the independent ensemble. This method becomes inefficient for too large entropies, which lead to very small N_A and large N_{\emptyset} . This is a problem of rare events which is also known in the related context of participation Rényi (PR) entropies^{26–28} and prohibits the estimation of large entropies in finite simulation time. The problem can however be cured by the application of the “ratio trick”^{14,29}, calculating the entanglement entropy by a stepwise increase of the subsystem A .

Let us give a description of the results presented in this article, along with its organization. We will first start from equation (2) to show how the measurement of the entanglement entropy is related to the basis dependent participation Rényi entropies $S_q^{PR,30}$ (also called Shannon-Rényi entropies in the litterature). The basic idea is to split the extended ensemble in its two parts and to simulate the ensemble of independent replicas and the ensemble of replicas that are glued together on subsystem A (see Fig. 1) separately. In Sec. II, we derive the following relation:

$$S_q^E = S_q^{PR} - C_q^R. \quad (3)$$

which relates the entanglement entropy S_q^E to the difference between participation Rényi entropy S_q^{PR} and the

replica correlation C_q^R , which is introduced in Sec. II and is defined in the glued ensemble.

Remarkably, this combination of two basis-dependent quantities will hint towards a more efficient calculation of the entanglement entropy, for two different reasons. First, large entanglement entropies can be obtained (both in our setup and the one used in Ref. 16) when using a QMC computational basis where the participation entropies S_q^{PR} are small. Second, we will introduce in Sec. III several improved Monte Carlo estimators which will greatly increase the precision on S_q^{PR} and consequently on S_q^E .

As an interesting by-product, our scheme allows to compute the thermodynamic Rényi entropy S_q^{th} in the specific case where the full system $\bar{\mathcal{O}}$ and the subsystem A are identical, as developed in Sec. IV. We will show there how the translation invariance in imaginary time can also be used to construct an improved estimator for the replica correlation C_q^R , leading to a very accurate result for the thermodynamic Rényi entropy. Let us emphasize that the thermodynamic Rényi entropy (for integer $q > 1$) can be calculated from two *standard* QMC simulations (using independent replicas) *without the need of implementing a different stochastic process or Wang-Landau sampling*.

The new methods are extensively tested and their efficiency discussed in Sec. V where we provide several results on quantum spin chains and ladders. We also explore in this section the possibility to reconstruct the entanglement spectrum from Rényi entanglement entropies^{19,31}, discussing the limitations of this approach. There, we also propose an alternative method to test a putative entanglement Hamiltonian, based on the comparison between Rényi entanglement entropies and the Rényi thermodynamic entropies of the entanglement Hamiltonian.

Finally, Sec. VI draws conclusions on our work while the appendices contain details on the improved estimator derivation as well as on using symmetry sectors when measuring entanglement entropies.

II. METHOD

The method proposed by Humeniuk and Roscilde¹⁶ uses an extended ensemble simulation (see Fig. 1), which dynamically moves between the glued ($\{A\}$) ensemble and the independent ensemble ($\{\emptyset\}$) and records the ratio of Monte Carlo steps performed in the glued *vs.* independent ensembles. For the equilibrium (Monte Carlo-) time t evolution of the probability $P_A(t)$ to be in ensemble A , the Master equation

$$\frac{dP_A(t)}{dt} = P_{\emptyset}(t)p_{\emptyset \rightarrow A} - P_A(t)p_{A \rightarrow \emptyset} \quad (4)$$

holds, where $p_{\emptyset \rightarrow A}$ is the probability of moving from the independent ensemble to the glued ensemble and $p_{A \rightarrow \emptyset}$ is the probability of the inverse move. In an equilibrated

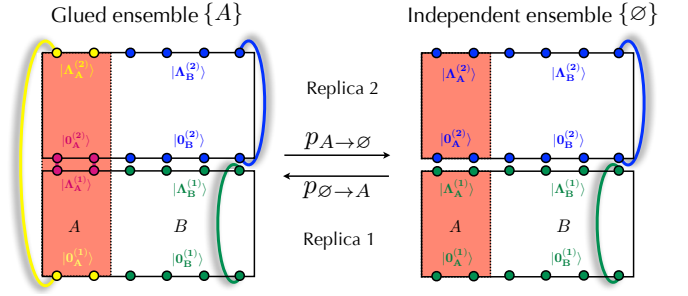


Figure 1: (Color online) Example of a QMC configuration with $q = 2$ replicas in the glued ensemble (left) and in the independent ensemble (right) with a notable difference of boundary conditions in imaginary time. Using the stochastic series expansion²² notations with operator strings of length Λ for illustration, these boundary conditions are as follows. Left: in the *glued ensemble*, the subsystem A state $|\Lambda_A^{(1)}\rangle$ at expansion slice Λ of replica 1 must be equal to $|0_A^{(2)}\rangle$ and consequently, $|\Lambda_A^{(2)}\rangle = |0_A^{(1)}\rangle$, while the operator string is Λ periodic in the subsystem B for each replica $\alpha \in \{1, 2\}$ (i.e. $|0_B^{(\alpha)}\rangle = |\Lambda_B^{(\alpha)}\rangle$). Right: the *independent ensemble* has the same cyclicity on subsystem B as in the glued ensemble but also shows the condition $|0_A^{(\alpha)}\rangle = |\Lambda_A^{(\alpha)}\rangle$ for all replicas on subsystem A . Therefore, all replicas are truly independent.

Markov chain of QMC configurations, the probability of finding the glued ensemble is time-independent, and we therefore obtain:

$$\frac{P_A}{P_{\emptyset}} = \frac{p_{\emptyset \rightarrow A}}{p_{A \rightarrow \emptyset}}. \quad (5)$$

and with equation (2)

$$S_q^E = \frac{1}{1-q} \ln \left(\frac{p_{\emptyset \rightarrow A}}{p_{A \rightarrow \emptyset}} \right). \quad (6)$$

Instead of calculating this ratio of probabilities in a single QMC calculation, let us now concentrate on an estimation of $p_{\emptyset \rightarrow A}$ and $p_{A \rightarrow \emptyset}$ in separate calculations.

A. Probability of leaving the independent ensemble $p_{\emptyset \rightarrow A}$

If the simulation is in the independent ensemble, the condition for moving to the glued ensemble is given by finding identical states on the subsystem A in all q replicas. This corresponds to identical states $|0_A^{(i)}\rangle$ for all replicas $i \in [1, 2, \dots, q]$ following the convention of Fig. 1. It is important to note that in principle due to the cyclicity of the trace the time slice where the replicas would be sewed together does not matter. However, we will not actually perform the step of moving to the glued ensemble here, but will just think about how probable it is. Clearly, we then have:

$$p_{\emptyset \rightarrow A} = P_{\text{identical}, q, A}. \quad (7)$$

But the probability $P_{\text{identical},q,A}$ of finding identical states on the subsystem A in all q replicas is just given by the participation Rényi entropies²⁶ of subsystem A

$$S_{A,q}^{\text{PR}} = \frac{1}{1-q} \ln P_{\text{identical},q,A}. \quad (8)$$

We will present in Sec. III improved estimators for estimating efficiently the participation Rényi entropies.

B. Probability of leaving the glued ensemble $p_{A \rightarrow \emptyset}$

When the simulation explores the glued ensemble $\{A\}$, the condition of moving to the independent ensemble is given by having identical states on top and bottom of each replica individually, such as to meet the condition of the trace. Therefore, $p_{A \rightarrow \emptyset}$ can be estimated by performing a simulation in the glued ensemble $\{A\}$ and recording how often this condition is met, relative to the total number of QMC steps. We have

$$p_{A \rightarrow \emptyset} = P_{\{A\}} \left(|0_A^{(1)}\rangle = |\Lambda_A^{(1)}\rangle \text{ and } \dots |0_A^{(q)}\rangle = |\Lambda_A^{(q)}\rangle \right). \quad (9)$$

This step turns out to be the bottleneck of the method in Ref. 16, as this probability decays exponentially with the number of degrees of freedom in the subsystem A and thus the *replica correlation*

$$C_{A,q}^{\text{R}} = \frac{1}{1-q} \ln p_{A \rightarrow \emptyset} \quad (10)$$

exhibits a *volume law*. Note that the participation Rényi part suffers similar exponentially small probabilities for which we can however improve the estimate (see Sec. III). This volume law is directly related to the problem of low acceptance rates in the standard method¹⁶. It should be noted that $C_{A,q}^{\text{R}}$ is not an entropy in the sense of equation (2) as in general no density matrix can be found that provides $C_{A,q}^{\text{R}}$ for all q . In particular, $C_{A,q}^{\text{R}}$ can grow with q , which is not possible for Rényi entropies.

C. Entanglement entropy

Combining the two results, we therefore arrive at the previously announced Eq. (3) for measuring entanglement entropies, which is restated for clarity using the spatial region index:

$$S_{A,q}^{\text{E}} = S_{A,q}^{\text{PR}} - C_{A,q}^{\text{R}}. \quad (11)$$

This relation between the Rényi form of the participation and entanglement entropies provides very interesting insights in the performance of any method based on the idea by Humeniuk and Roscilde¹⁶. It has been established that PR entropies show a volume law in local bases,^{26–28,30,32,33}. However the coefficient of the volume term is non-universal and depends on the basis.

As entanglement entropies usually display an *area law* for condensed-matter ground-states³⁴, the replica correlation $C_{A,q}^{\text{R}}$ necessarily has to exhibit the same volume law (and correspondingly, the probability to leave the glued ensemble decreases exponentially with the number of degrees of freedom in A).

The same reasoning goes for the basis dependence: $S_{A,q}^{\text{PR}}$ depends on the basis, while $S_{A,q}^{\text{E}}$ *does not*. Thus, $C_{A,q}^{\text{R}}$ needs to be a basis dependent quantity, too. As the probabilities to be observed in the QMC calculations are potentially very small, it is beneficial to choose the basis in which they assume *larger* values. Therefore, one should try to choose a computational basis in which the participation entropy $S_{A,q}^{\text{PR}}$ is the *smallest*. One notable example is a simulation of the XX model $H_{\text{XX}} = \sum_{\langle i,j \rangle} S_i^x S_j^x + S_i^y S_j^y$ in the basis in which S_x is diagonal instead of the usual S_z basis.

III. IMPROVED ESTIMATORS

Too large entropies lead in general to statistical issues in the QMC simulations. In order to tackle problems connected to the corresponding rare events, it is useful to increase the number of Monte Carlo measurements as much as possible. Here, we present improved estimators that greatly enhance the precision of participation entropies S_q^{PR} using all possible symmetries in imaginary time and real space.

The starting point is the replica method introduced in Ref. 26. The basic idea is that in order to measure the PR entropy S_q^{PR} of a subsystem A (which may coincide with the full system), it is sufficient to estimate the probability of finding the same state $|i\rangle_A$ on the part corresponding to subsystem A of the state at operator string slice i . According to the convention given in Fig. 1, this corresponds to the estimator

$$\langle p_{\emptyset \rightarrow A}^{(q)} \rangle_{\text{MC}} = \frac{1}{N_{\text{MC}}} \sum_{\text{MC}} \frac{1}{\Lambda} \sum_i \delta_{|i_A^{(1)}\rangle, |i_A^{(2)}\rangle} \dots \delta_{|i_A^{(q-1)}\rangle, |i_A^{(q)}\rangle}, \quad (12)$$

where the first sum runs over the Markov chain of length N_{MC} and the second sum over all Λ slices i of the operator strings in the q replicas. For simplicity, we enforce the same cutoff Λ for all replicas.

This method can be greatly enhanced by the observation that all operator strings in the ensemble $\{\emptyset\}$ are *independent*. This leads to two possible improvements:

- Due to the cyclicity of the trace, each operator string has a cylinder topology and can thus be independently translated cyclically by any number of states in the “imaginary time” direction. Each of the such transformed Monte Carlo configurations has exactly the same weight.
- If the system is invariant under (spatial) symmetry transformations, we can transform the *whole* oper-

ator string of each replica with *independent* transformations without changing the weight of the configuration.

These two recipes can be used to greatly improve the quality of the estimation of S_q^{PR} . However, a naive application of these ideas is not possible as it is far too expensive to try all combinations of shifted and transformed operator strings. As discussed below, it is possible to exploit all symmetries by only one pass on each operator string.

A. PR entropy of the full system $A = \overline{\emptyset}$

Let us first start with the full system $A = \overline{\emptyset}$ as the symmetries are simpler to apply and the resulting improved estimator formulae are clearer.

For each state $|i^{(\alpha)}\rangle$ in the operator string of replica α , we calculate the parent state $p(|i^{(\alpha)}\rangle)$ by applying all model symmetries. The application of all symmetries classes all the basis states $|i\rangle$ into *nonoverlapping* families of states, each of which is represented by the uniquely defined parent state – here, we will take the state in the family with the smallest binary representation. It is important to record the multiplicity (*i.e.* the number of states belonging to the family) $d(|p\rangle)$ of each state family for the purpose of correct normalization. Note that most state families have the maximal multiplicity given by the number of symmetries n_{sym} , with the exception of high symmetry states for which $d < n_{\text{sym}}$.

While transversing all the operator strings, we record the histogram $h = \{n(|p\rangle, \alpha)\}$ of the number of occurrences $n(|p\rangle, \alpha)$ of states with parent $|p\rangle$ in operator string α .

In the next step, for each parent state that has been observed in one of the replicas we have to count the number of configurations (of symmetry-transformed operator strings) in which we can find identical states in all q replicas. It is clearly given by

$$n_{\text{id}}(|p\rangle) = d(|p\rangle) \prod_{\alpha=1}^q n(|p\rangle, \alpha). \quad (13)$$

Note that the multiplicity $d(|p\rangle)$ of the parent state $|p\rangle$ accounts for the fact that we can have any of the $d(|p\rangle)$ states in the family of parent $|p\rangle$ as the identical state in all replicas.

Finally, we have to normalize equation (13) by the total number of symmetry equivalent configurations of all q replicas. As the family of parent $|p\rangle$ consists of $d(|p\rangle)$ states, the correct normalization is $\frac{1}{d(|p\rangle)^q}$. Together with the Λ^q possible cyclical shifts of the operator strings, this yields the improved estimator in Monte Carlo configuration \mathcal{C} for the probability of moving from the independent $\{\emptyset\}$ ensemble to the glued ensemble $\{A\}$

$$\langle\langle p_{\emptyset \rightarrow \overline{\emptyset}}^{(q)} \rangle\rangle_{\mathcal{C}} = \frac{1}{\Lambda^q} \sum_{|p\rangle \in h} d(|p\rangle)^{1-q} \prod_{\alpha=1}^q n(|p\rangle, \alpha). \quad (14)$$

Here, Λ is the number of states in the operator string (forced to be equal in all replicas for simplicity). The sum runs over all parent states recorded in the histogram h . In equation (14) it is immediately clear why this method is extremely beneficial for the observation of small probabilities: the normalization factor can become a very small number, as typically the number of applied symmetries $\approx N$ for a translationally invariant system with N sites and $\Lambda \approx 10^3 \dots 10^5$ in our calculations. For large values of q , very small numbers can be obtained by *one* Monte Carlo measurement and the variance of the estimator is greatly reduced.

Because of the tremendous number of possible combinations of symmetry transformed replica operator strings, it should be noted that the evaluation of Eq. (14) may cause numerical problems. The products of the numbers $n(|p\rangle, \alpha)$ for all q replicas can easily become too large to be stored as 64-bit integers. One solution for this problem is to use extended precision floating point numbers. We have found, however, that it is sufficient to perform the products using double precision floating point numbers and performing the sum using Kahan's summation algorithm³⁵ to avoid precision loss and cancellation effects.

An interesting further improvement of the method stems from the fact that a *single* simulation of q_{max} replicas can be used for the calculations of PR entropies $S_{A,q}^{\text{PR}}$ (or equivalently the probabilities $p_{\emptyset \rightarrow A}^{(q)}$) with q ranging from 2 to q_{max} . Indeed, at the time of performing a Monte Carlo measurement, we can select any combination (without repetition) of q replicas out of the q_{max} copies and apply Eq. (14) without the need of creating a new histogram. This can be repeated for all $\binom{q_{\text{max}}}{q} = \frac{q_{\text{max}}!}{q!(q_{\text{max}}-q)!}$ possibilities, further improving the precision of the estimate:

$$\langle\langle p_{\emptyset \rightarrow \overline{\emptyset}}^{(q)} \rangle\rangle_{\mathcal{C}} = \frac{1}{\binom{q_{\text{max}}}{q}} \frac{1}{\Lambda^q} \times \sum_{|p\rangle \in h} d(|p\rangle)^{1-q} \sum_{\gamma} \prod_{\alpha=1}^q n(|p\rangle, \gamma(\alpha)). \quad (15)$$

where the additional sum runs over all combinations γ of the q_{max} replicas.

B. PR entropy of subsystem A

If the subsystem A and the full system are not identical, we have to slightly modify the procedure described above. The reason for this is the fact that if we cut out the part of subsystem A from every state in the family corresponding to a parent $|p\rangle$ and for a different family corresponding to $|p'\rangle$, we will find that the families can now have an overlap if the full system has more or different symmetries than the subsystem, which is generally the case. In some cases, where the exploited symmetries

of the subsystem are identical with the symmetries of the full system, the same algorithm as for the full system may be used. This is generally the case if any symmetry transformation maps the subsystem on itself, *e.g.* in the case of the periodic ladder (see below, Sec. VB) when solely using translation symmetries along the ladder.

In the general case, accounting for these overlaps is expensive as all pairs of parent states in the histogram h have to be treated. We therefore choose to go through all parents in the histogram h and create the family of states from which we deduce the subsystem states $|i\rangle_A$ by cutting out the corresponding part. In doing so, we generate a new histogram h_A filled with the cut states $|i\rangle_A$ where we accumulate the corresponding $n(|p\rangle, \alpha)$ from histogram h . Note that the histogram h_A may become very large if the number of symmetries and the number of lattice sites in subsystem A is large. The size of the histogram h is always smaller or at most equal to $q_{\max}\Lambda$ (typically, its size is reduced by the number n_{sym} of symmetries to $q_{\max}\Lambda/n_{\text{sym}}$). The maximal size of the histogram h_A is, however, given by $\max(n_{\text{sym}}q_{\max}\Lambda, \mathcal{N}_A)$, where \mathcal{N}_A is the dimension of the Hilbert space of states on subsystem A . Note that the relevant number of symmetries n_{sym} here is the number of applied symmetries of the full system as we discuss here the general case, in which the subsystem has no (or less) symmetries.

The equation for the estimator in the previous section only have to be slightly modified:

$$\sum_{|p\rangle \in h} d(|p\rangle)^{1-q} \rightarrow \frac{1}{n_{\text{sym}}} \sum_{|i\rangle_A \in h_A}, \quad \text{and} \quad |p\rangle \rightarrow |i\rangle_A, \quad (16)$$

where $n(|i\rangle_A, \alpha)$ is then the number of times the subsystem state $|i\rangle_A$ has been observed in all symmetry realizations of replica α . This yields the final estimator

$$\langle \langle p_{\emptyset \rightarrow A}^{(q)} \rangle \rangle_c = \frac{1}{\binom{q_{\max}}{q}} \frac{1}{(n_{\text{sym}}\Lambda)^q} \times \sum_{|i\rangle_A \in h_A} \sum_{\gamma} \prod_{\alpha=1}^q n(|i\rangle_A, \gamma(\alpha)). \quad (17)$$

C. Autocorrelation problem for large values of q

While the improved estimator performs remarkably well for a wide range of q and compares perfectly with exact results for small systems (see Sec. V), we have found that it may yield wrong results for large values of q in some extreme cases. A detailed investigation shows that this behavior stems from an increasing variance of the improved estimator with q together with an increasing autocorrelation time which may exceed the simulation time and thus yield systematic errors⁵⁰.

The reason for this behavior is identified by studying the time series of the estimator for different values of q (see Fig. 2). Clearly, for larger values of q , the time series shows more and more pronounced “spikes” that at the

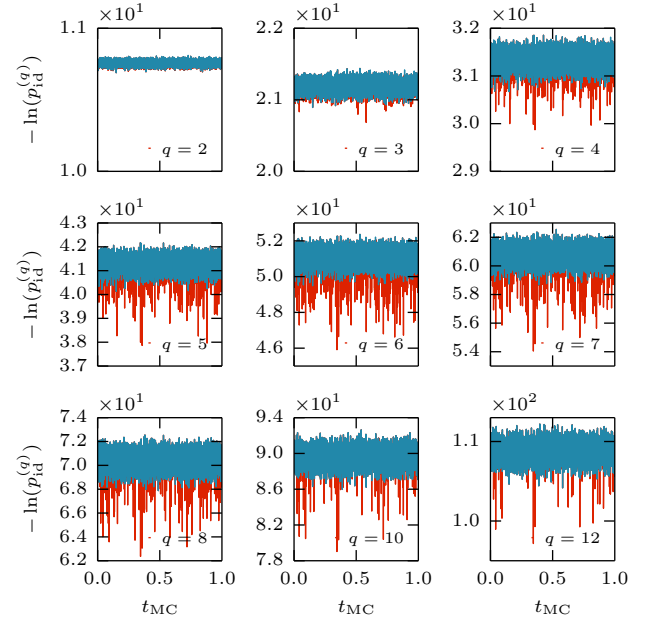


Figure 2: (Color online) Comparison of the time series of (minus log of) the estimator given by Eq. (17) (shown in red) and the estimator excluding the most probable states (shown in blue) for different Rényi indices q for the $L = 16$ Heisenberg ladder at $J_{\perp} = 4$. Clearly, the variance of the estimator excluding the most probable states is very much reduced.

same time become rare and large for large q . We have found that the most severe spikes are created by the occurrence of the most probable states (for antiferromagnetic systems, these are the Néel states $|N_A\rangle$ and $|N_B\rangle$, see Refs. 26–28). These states occur with the highest probability p_{\max} in any operator string and have an enhanced symmetry (for instance the symmetry family of the Néel states only has a $d = 2$ multiplicity). Consequently, the factor $d(|p\rangle)^{1-q}$ in Eq. (15) is much larger than for less symmetric states (for which it is usually n_{sym}^{1-q}), creating extremely large spikes for large q if the Néel states are observed in all q replicas simultaneously. The frequency of the spikes becomes however rare with growing q , as the simultaneous observation probability of the Néel states in all q replicas decreases rapidly as p_{\max}^q .

However, we can remedy this situation by calculating the probability p_{\max} separately, recording the frequency of the Néel states across all replicas. We then deliberately exclude the most probable states with common parent $|N_A\rangle = p(|N_A\rangle) = p(|N_B\rangle)$ from the estimator in Eq. (15) (similarly for Eq. (17)) and obtain

$$\langle \langle p_{\emptyset \rightarrow \emptyset}^{(q)} \rangle \rangle_c = \frac{1}{\binom{q_{\max}}{q}} \frac{1}{\Lambda^q} \times \sum_{|p\rangle \in h, |p\rangle \neq |N_A\rangle} \left[d(|p\rangle)^{1-q} \sum_{\gamma} \prod_{\alpha=1}^q n(|p\rangle, \gamma(\alpha)) \right] + d(|N_A\rangle) p_{\max}^q. \quad (18)$$

In order to pull out the term $d(|N_A\rangle)p_{\max}^q$ out of the sum, we have used the fact that on average the frequency $n(p(|N_A\rangle), \alpha)$ of the Néel states in replica α of length Λ is given by $\Lambda d(p(|N_A\rangle))p_{\max}$.

In Fig. 2, we compare the time series of (minus log of) the estimator given by Eq. (15) and the improved estimator (excluding the additive term $+d(|N_A\rangle)p_{\max}^q$) given by Eq. (18) in a test example discussed deeper later. Clearly, for $q = 2$ the two estimators behave nearly exactly equally. However, as q grows, the estimator not excluding the most probable states (shown in red) has a much larger variance than the estimator that excludes the most probable state. In addition to that, the spikes created by the Néel state become rare with growing q and eventually may not be even recorded once in a simulation, leading to incorrect results (especially since p_{\max} will dominate the PR entropy for large values of q).

Note that usually p_{\max} can be calculated with a much higher precision than any other state, leaving us with the possibility to correct efficiently this systematic error. Any other state can be taken out of the estimator as in Eq. (18) if its probability can be measured to a sufficient accuracy directly. This way, a hybrid method capturing the histogram of the most probable states with high precision and calculating the correction caused by the less probable states by the replica trick can be easily constructed.

D. Measurement of the replica correlation entropy

The final element to compute the entanglement entropy is the measurement of the replica correlation entropy $C_{A,q}^R$, for which the probability $p_{A \rightarrow \emptyset}$ has to be estimated efficiently.

In the method of Ref. 16, the condition for moving from the glued ensemble to the independent ensemble is given by $|0_A^{(2)}\rangle = |0_A^{(1)}\rangle$. In this case, the glue can be cut and rewired thus moving from the glued to the independent ensemble *without changing the weight* as illustrated in Fig. 1.

In our scheme, we can simply simulate the glued ensemble and measure the number of times we observe $|0_A^{(2)}\rangle = |0_A^{(1)}\rangle$ relative to the total number of QMC steps. Unfortunately, the glued replicas can not be changed by separate symmetry transformations and the topology of the glued operator string is rigid in imaginary time, *i.e.* it can not be translated. Generally, it is therefore not possible to construct an improved estimators for $C_{A,q}^R$ in the same way as for $S_{A,q}^{\text{PR}}$.

IV. THERMODYNAMIC RÉNYI ENTROPIES

Let us discuss in more detail the special case in which the subsystem A and the full system $\overline{\mathcal{O}}$ are identical. In that case, the entanglement Rényi entropies S_q^E reduce

to the thermodynamic Rényi entropies $S_q(\beta)$ at inverse temperature β , which are defined by:

$$\begin{aligned} S_q^{\text{th}}(\beta) &= \frac{1}{1-q} \ln \frac{\text{Tr } e^{-q\beta\hat{H}}}{\left(\text{Tr } e^{-\beta\hat{H}}\right)^q} \\ &= \frac{q\beta}{1-q} [F(\beta) - F(q\beta)]. \end{aligned} \quad (19)$$

Here, $F(\beta) = -\frac{1}{\beta} \ln \text{Tr } e^{-\beta\hat{H}}$ denotes the free energy of the system governed by the Hamiltonian \hat{H} at inverse temperature β . Noting that the thermal density matrix $\rho_{\overline{\mathcal{O}}}$ is nothing else but the reduced density matrix of the subsystem $A = \overline{\mathcal{O}}$, we can use Eq. (3) to calculate the thermodynamic Rényi entropy.

As in the case of the entanglement Rényi entropy, we will decompose the thermodynamic Rényi entropy in a difference of the participation PR entropy and the replica correlation. The discussion of Sec. III on how to build improved estimators exploiting spatial and imaginary time symmetries carries on for the calculation of the PR entropy.

The calculation of the replica correlation for $A = \overline{\mathcal{O}}$ can be much further improved than in the generic case. Indeed this is the case where the replicas are glued on the full system and the periodicity in β (or in the cutoff Λ for SSE) is replaced by a $q\beta$ periodicity for a larger operator string. Clearly, this situation can be achieved by simply performing a standard SSE simulation with a *single replica* at inverse temperature $q\beta$. The estimator for the replica correlation C_q^R is then given by the probability of cutting the enlarged configurations in q valid SSE replicas at inverse temperatures β , with the condition that these q replicas have to be periodic in β .

It should be observed that there are multiple valid ways of slicing the large configuration in q parts and in fact any partition $(\Lambda_1, \dots, \Lambda_q)$ is valid *as long as every cutoff Λ_i is large enough such as to correctly sample the inverse temperature β* . The probability of slicing the large replica in q valid parts can be estimated (see Appendix A for a detailed derivation) by simply measuring the observable

$$X_{\overline{\mathcal{O}} \rightarrow \emptyset} = \delta_{\alpha_1, \Lambda_1, \dots, \alpha_q, \Lambda_q} \frac{\Lambda! \prod_{i=1}^q (\Lambda_i - n_i)!}{q^n (\Lambda - n)! \prod_{i=1}^q \Lambda_i!} \quad (20)$$

for any Monte Carlo configuration in the replica simulated at inverse temperature $q\beta$. Here, the Kronecker delta yields 1 if the states α_i at the beginning of each replica of length Λ_i are identical, which is precisely the condition for obtaining q valid, Λ_i -periodic replicas after performing the cut. Note that one should of course average over several possible partitions $(\Lambda_1, \dots, \Lambda_q)$ with $\Lambda = \sum_i \Lambda_i$ and all translations of the partitions in imaginary time.

We obtain

$$C_q^R = \frac{1}{1-q} \ln(\langle X_{\overline{\mathcal{O}} \rightarrow \emptyset} \rangle_{\text{MC}, \{\Lambda_i\}}) \quad (21)$$

where the average is performed over the Markov chain and different partitions in order to improve the statistics. The thermodynamic Rényi entropy is thus finally given by

$$S_q^{\text{th}} = S_q^{\text{PR}} - C_q^{\text{R}}, \quad (22)$$

where the absence of the subsystem index indicates that the full system is to be considered. We emphasize that both S_q^{PR} and C_q^{R} are obtained within a standard SSE independent ensemble simulation.

V. RESULTS

In this section we present various results obtained on simple model Hamiltonians, such as Heisenberg chains and ladders, in order to carefully test the method. We compare, when possible, our QMC estimates with exact diagonalization (ED) or DMRG results. The quantities of interest we discuss in the rest are the Rényi entanglement (zero temperature) and thermodynamic (finite temperature) entropies. We also compare the efficiency of our new method for calculating entanglement entropies $S_{A,q}^{\text{E}}$ with the method of Ref. 16.

The last part of this section deals with a careful analysis of the reconstruction of the entanglement spectrum given entanglement entropies. We finally provide a quantitative analysis of how to probe an ansatz entanglement Hamiltonian in the case of Heisenberg ladders.

A. Heisenberg chain

As a first application of the different aspects of the method introduced in Sec. II we perform calculations for the well-studied antiferromagnetic Heisenberg chain of L spins $S = \frac{1}{2}$, described by the Hamiltonian

$$H_{\text{1d}} = J \sum_i \vec{S}_i \cdot \vec{S}_{i+1}, \quad (23)$$

using periodic boundary conditions $\vec{S}_{L+1} = \vec{S}_1$.

1. Entanglement entropies

We test our implementation on the example of a chain of $L = 16$ spins, which can be easily solved using ED. As a way to show the different elements in our method, we first display in the main panel of Fig. 3 the participation entropies S_q^{PR} as a function of the subsystem size ℓ and Rényi index q . The correspondence between the QMC and exact result is perfect and the precision is such that the error bars are not even visible in the graph. The inset displays the probabilities $p_{\text{id}}^{(q)}$ of finding the same basis state in q replicas for q ranging from 2 to 10, for the full system $\ell = L$. The exponential decay

of $p_{\text{id}}^{(q)} = \exp[-(q-1)S_q^{\text{PR}}]$ is perfectly reproduced by the Monte Carlo result and even the smallest probabilities of the order of 10^{-27} are estimated with extremely high accuracy (errorbar of the order of 10^{-29}) in a calculation containing 10^6 Monte Carlo measures. In order to appreciate this result, let us mention that the simple estimator given in Eq. (12) can hardly see a single event occurring with such low probabilities. The reason for this is that the total denominator $N_{\text{MC}}n$ for the present case is given by $N_{\text{MC}} = 10^6$ and the expansion order $\langle n \rangle = 3553.08(5)$ (for the case of $L = 32$), thus it is of the order of 10^9 . Consequently, events of probabilities $p < 10^{-9}$ will typically never be seen in a Markov chain of length $N_{\text{MC}} \approx 10^6$.

Let us now combine the result in Fig. 3 with the result for the calculation of the replica correlation entropy to obtain the entanglement Rényi entropy according to equation (3). Fig. 4 shows the comparison of this result with the one obtained by ED. The correspondence is again perfect and shows that the method works very well: for instance, the even-odd oscillations for $q \geq 2$ are perfectly reproduced³⁶. Note that the errorbars of the two Monte Carlo results yield the final error of S_q^{E} by

$$\sigma_{\text{E}} = \sqrt{\sigma_{\text{PR}}^2 + \sigma_{\text{R}}^2}. \quad (24)$$

We usually find that the error bar of the replica correlation entropy σ_{R} is larger than the error of the PR entropy

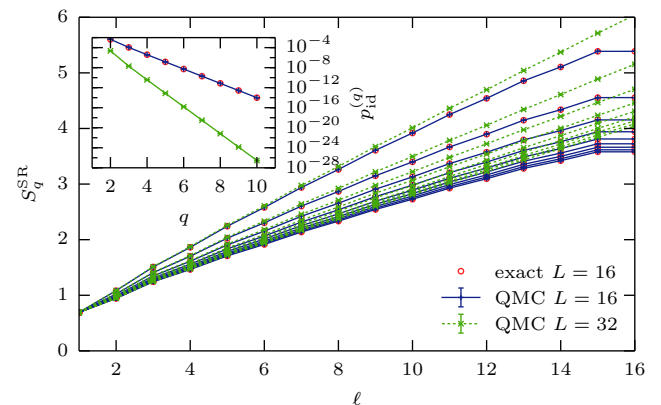


Figure 3: (Color online) QMC results for the $L = 16$ and $L = 32$ Heisenberg chains. We also show the comparison to the exact solution obtained by exact diagonalization for $L = 16$. The main panel shows the PR entropy S_q^{PR} as a function of subsystem size ℓ for $q = 2, 3 \dots 10$, where $q = 2$ corresponds to the largest entropies and $q = 10$ to the smallest ones. In the inset, we display the corresponding probability $p_{\text{id}}^{(q)}$ of finding the same state for the full system $\ell = L$ in all q replicas. The QMC results stem from 10^6 Monte Carlo measurements and the average expansion order was $\langle n \rangle = 891.36(2)$ for $L = 16$ and $\langle n \rangle = 3553.08(5)$ for $L = 32$. Using a simple average over all imaginary time slices, one would be blind to probabilities $p \lesssim 10^{-9}$. With our improved method, we not only are able to calculate *much* smaller probabilities, but also obtain a very small variance of the result.

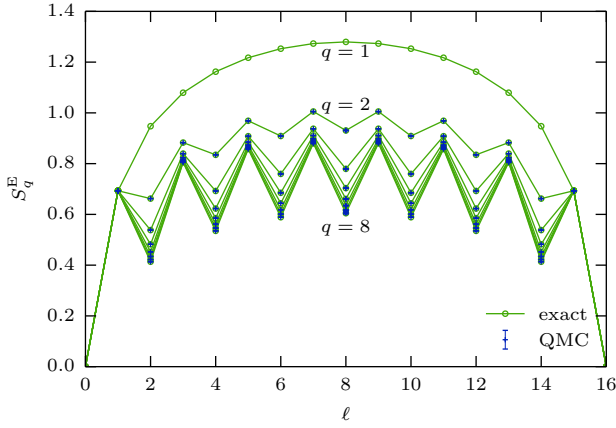


Figure 4: (Color online) QMC results for the entanglement Rényi entropies S_q^E for a bipartition of the $L = 16$ Heisenberg chain as a function of subsystem size ℓ compared to exact diagonalization. The Monte Carlo results have been obtained from Eq. (3) and have been symmetrized around $\ell = L/2$. The $q = 1$ result is not accessible from a Monte Carlo calculation and is included for illustration purposes.

σ_{PR} due to the lack of an improved estimator of C_q^R and therefore dominates the total error.

2. Thermodynamic Rényi entropies

We here now consider the full-system made of the chain to obtain the thermodynamic Rényi entropy. We have performed calculations with $q = 2, 3$ replicas for the periodic Heisenberg chain at different finite temperature for different system sizes and calculated the participation entropies $S_q^{PR}(\beta)$. A second set of simulations at inverse temperatures $q\beta$ has then been carried out in order to obtain the replica correlation C_q^R using Eq. (21). We extracted the thermodynamic Rényi entropies $S_2^{th}(\beta)$ and $S_3^{th}(\beta)$ from the result and compare to ED in Figure 5. Clearly the QMC result for $L = 20$ matches the exact values perfectly. Furthermore, one can access much larger chain sizes as compared to ED techniques, limited to $L \sim 20$ for the full diagonalization required to access finite temperature behaviour.

We also show the temperature dependence of the individual terms (see inset of Fig. 5) from which the thermodynamic Rényi entropy is obtained. While the participation entropy decreases with inverse temperature (it assumes its maximal value of $L \ln 2$ at $\beta = 0$), the replica correlation increases to eventually match the value of the PR entropy at zero temperature.

One can also test with $S = 1/2$ chains the conformal field theory prediction for $S_q^{th}(\beta)$. In the regime $1 \ll u\beta \ll L$ (and ignoring logarithmic corrections due to marginal operators³⁷), the free energy obeys the following

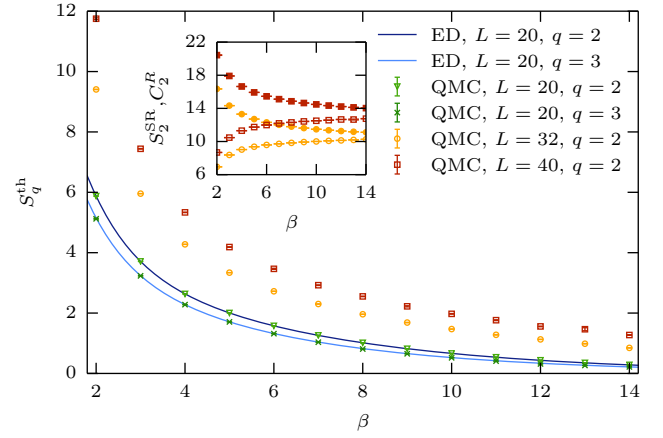


Figure 5: (Color online) Thermodynamic Rényi entropies obtained from Monte Carlo simulations. The match with the exact diagonalization result is perfect. The inset shows the dependence of the participation entropy (filled symbols) and the replica correlation (open symbols) on the inverse temperature β for $L = 32$ (yellow circles) and $L = 40$ (red squares).

scaling³⁸

$$F(T) = E_0 - L \frac{\pi c}{6u} T^2, \quad (25)$$

where E_0 is the ground-state energy, c the central charge, and u the velocity of excitations. Using Eq. (19), one arrives for the low temperature scaling to:

$$S_q^{th}(T) = \frac{\pi c}{6u} \left(1 + \frac{1}{q}\right) LT. \quad (26)$$

This behavior is checked with $q = 2$ for XXX chains of various lengths $L = 20, 32, 40$ in Fig. 6 (left), where the low temperature linear form is well reproduced using $c = 1$ and $u = \pi/2$. Finite size convergence effects are

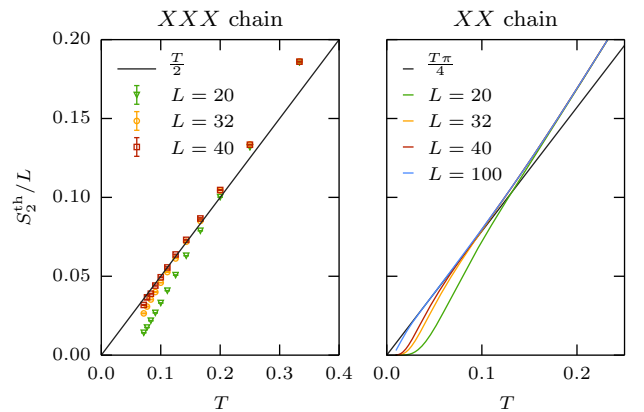


Figure 6: (Color online) Thermodynamic Rényi entropies for the XXX (QMC left) and XX (ED right) chains compared to the low temperatures CFT prediction Eq. (26).

due to the finite length gap $G(L) \simeq u/L$ such that the asymptotic low T behavior Eq. (26) is expected to be valid for $u \gg T \gg G(L)$. Below this gap, S_q^{th} displays an activated shape, controlled by $G(L)$. We checked this finite-size effect using ED at the free-fermion point (XX chain) with open boundary conditions⁵¹ where the asymptotic linear scaling is perfectly well reproduced for large enough sizes L , as displayed in Fig. 6 (right).

B. Heisenberg ladders

Let us now consider Heisenberg ladders consisting of two neighboring one dimensional periodic Heisenberg chains (the “legs”) with an additional “rung” coupling between the chains:

$$H_{\text{ladder}} = J \sum_{i,\alpha} \vec{S}_{i,\alpha} \cdot \vec{S}_{i+1,\alpha} + J_{\perp} \sum_i \vec{S}_{i,\ell} \cdot \vec{S}_{i,r}. \quad (27)$$

where $\vec{S}_{i,\alpha}$ is the spin operator on site i of chain $\alpha = \ell, r$, corresponding to the left and right leg respectively (see Fig. 7). We use periodic boundary conditions along the legs.

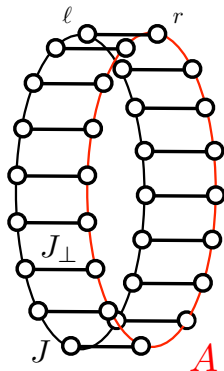


Figure 7: (Color online) Schematic picture for the spin ladder system Eq. (27). Entanglement is studied between subsystem A (red) and the rest.

For the calculation of entanglement properties, we consider the cut where A is one leg of the ladder and perform calculations in the strongly gapped rung-singlet regime $J_{\perp} \gg J$, where entanglement entropies are known to be quite large from ED studies^{39,40}. The motivation for this regime is to test our method in a difficult, large-entanglement, regime. Such a cut has also been used in several other works on ladder systems^{39–46}.

1. Entanglement entropies

Fig. 8 displays our QMC result for various values of q , system sizes ranging from $L = 10$ to $L = 32$ and $J_{\perp} = 4J$.

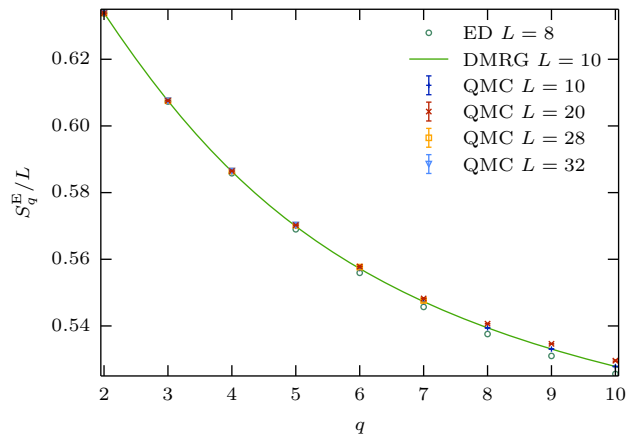


Figure 8: (Color online) Entanglement Rényi entropies S_q^E for different Rényi indices q for the ladder with $J_{\perp} = 4$. For the ladder consisting of $L = 10$ rungs, we also add the numerically exact DMRG result for comparison. Note that for this particularly strongly entangled system, DMRG can in fact access systems up to $L \approx 16$ which corresponds to the limit of ED³⁹. Our QMC calculation can go further and begins to show problems because of too large autocorrelation times around $L = 32$ for $q > 5$.

For comparison, we also display the numerically exact DMRG result for $L = 10$. We are still able to perform the calculation for q up to as large as $q_{\text{max}} = 10$ for $L = 20$ and begin to see limitations at $q = 7$ for $L = 28$ as the errorbar becomes larger. Clearly, the situation becomes worse for $L = 32$, while the result for smaller values of q remains extremely good. For comparison, ED (due to the Hilbert space size) or DMRG (due to the large entanglement in this regime) cannot reach systems larger than $L \approx 16$.

Interestingly, the finite size effects on $S_{A,q}^E/L$ strongly depend on the Rényi index q . For $q = 2$, no difference between the result for $L = 8$ and the one for $L = 32$ is visible, however, for $q \geq 7$, $S_{A,q}^E/L$ displays a sizeable finite length L dependence. This can be easily understood if one realizes that the Rényi index q plays the role of an inverse temperature in the entanglement spectrum. This behavior points to a stronger finite size dependence of the lowest lying level of the entanglement spectrum (*i.e.* the groundstate energy of the entanglement Hamiltonian — see discussion later) than for high temperature quantities, which are averaged over the whole spectrum.

2. Comparison with the mixed ensemble method

In order to get an estimate of the efficiency of the method discussed in this article, we performed calculations for the $L = 20$, $J_{\perp} = 4$ Heisenberg ladder, where subsystem A corresponds to one leg of the ladder (Fig. 7), and compare to results obtained using the method of Humeniuk and Roscilde¹⁶ where for every q , we optimized

q	S_q^E (ratio trick)	S_q^E (from PR)
2	12.67691 ± 0.00031	12.676998 ± 0.000026
3	12.15135 ± 0.00040	12.151270 ± 0.000040
6	11.15622 ± 0.00076	11.156525 ± 0.000394
10	10.58810 ± 0.00201	10.590639 ± 0.005246

Table I: Entanglement entropy of the $L = 20$, $J_\perp = 4$ Heisenberg ladder as calculated using the method described in Ref. 16 (left column) and using the method presented in this article (right column). For both calculations we used the same total amount of CPU time on the same computer. Note that for $q = 2$ and $q = 3$, our proposed method reduces the errorbar of the result by roughly a factor of 10, while for $q = 10$, the ratio trick becomes more efficient.

the subsystem increment used for the ratio trick¹⁴.

Using the same amount of CPU time (80% for C_q^R and 20% for S_q^{PR} for our method), we compare the values of the errorbars between the two different methods. The results are shown in Table I. Clearly, for small values of q , the error bars obtained from our method are reduced by one order of magnitude. For very large values of q , the situation changes and the ratio trick provides a better accuracy, leading to an errorbar that is roughly 2.5 times smaller. This comes from the fact that computing the replica correlation C_q^R part scales exponentially with q , and, as it was explained previously, no improved estimator is available. For practical purposes, it means that we are limited to values of q such that $p_{A \rightarrow \emptyset} \gtrsim 10^{-7}$ (corresponding to $q = 10$ in this particular case) and the associated error will dominate the total error. On the other hand, in the mixed ensemble calculation the ratio trick offers some flexibility in a certain range of q . For $q = 2$, the best error bar is generally obtained for an increment larger than one, whereas for larger q it becomes quickly much more efficient to set it to unity. Thus, it becomes computationally more interesting to make several simulations for which the probabilities are larger, yielding an exponential gain, while the cpu time required by the increasing number of simulations in order to maintain a constant error bar increases as l^2 (l the number of increments). This explains why the mixed ensemble method¹⁶ becomes more efficient when q grows.

It should be noted that this comparison is rather rough, as all three implementations have slightly different optimization goals. Additionally, we did not optimize the CPU time ratio between the calculation of C_q^R and S_q^{PR} , which can certainly lead to some improvement. For the calculation of S_q^{PR} we used 10 replicas and obtained the result for $q = 2, 3, \dots, 10$ in one single simulation, while in the other two simulations, every q has to be done separately. Therefore the comparison gives a slight advantage to the method of Humeniuk and Roscilde as the S_q^{PR} calculation provides more information (on $q = 4, 5, 7, 8$ and 9) than needed.

Let us finally mention that the biggest advantage of

the method proposed in this article is found in situations of very large entropies, such as the example of the ladders presented here. For the case of weak entanglement entropies such as the one dimensional Heisenberg chain, we obtained roughly the same errorbars in both methods for $q = 2$, indicating that the mixed ensemble method performs very efficiently here.

C. Entanglement spectrum reconstruction

Having access to the entanglement entropies for various values of the Rényi index, we are able to explore a recently proposed method for the reconstruction of the entanglement spectrum from Rényi entanglement entropies measured in QMC^{19,31}. The method relies on the Newton-Girard identities, linking the coefficients of a polynomial to the power sums of its roots. This means that a polynomial with roots at the λ_i corresponding to the entanglement spectrum can be constructed from the knowledge of Rényi entanglement entropies (λ_i are the eigenvalues of the reduced density matrix).

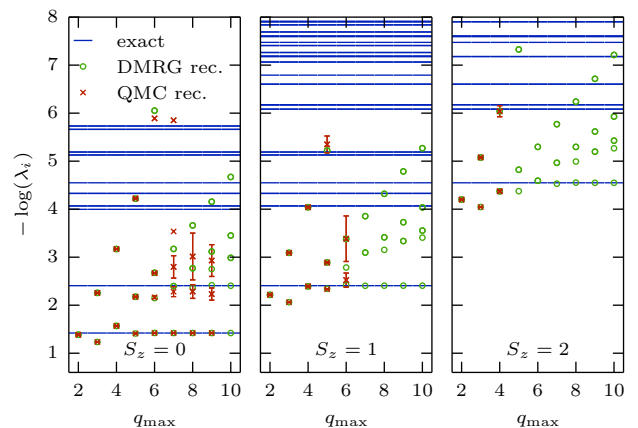


Figure 9: (Color online) Reconstructed entanglement spectrum for the $L = 10$ Heisenberg ladder at $J_\perp = 1$ as a function of q_{\max} . We have separated the spectrum in symmetry sectors of S_z similar to Ref. 19 and display the exact spectrum obtained from a DMRG calculation for reference. In addition to the reconstructed spectrum from our QMC data, we also reconstruct the entanglement spectrum from the exact DMRG entanglement entropies in each sector in order to study the role of the statistical errors. We have performed the reconstruction for different cutoffs q_{\max} corresponding to the maximal Rényi index involved in the reconstruction. Errorbars stem from a bootstrap analysis of QMC data.

However, in a practical QMC calculation, the Rényi entanglement entropies are neither known for arbitrarily many values of q nor to unlimited precision. Therefore, the polynomial has to be truncated and its order is limited to the maximal Rényi index q_{\max} . For the one-dimensional extended Bose-Hubbard model, Chung *et al.*¹⁹ obtained interesting results for the low lying en-

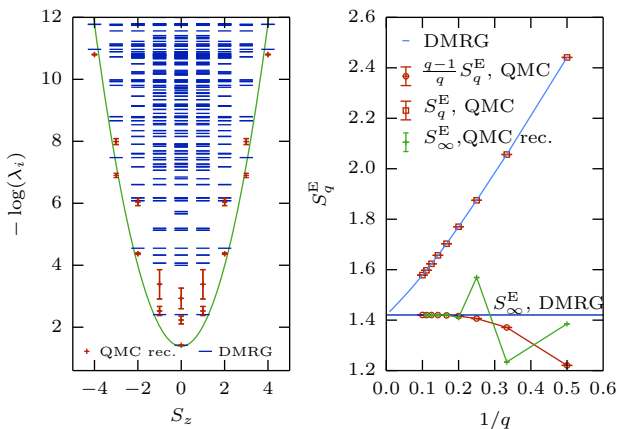


Figure 10: Left: Entanglement spectrum for the $J_{\perp} = 1$ Heisenberg ladder of length $L = 10$ obtained from DMRG and resolved by symmetry sectors of S_z . The parabolic envelope is a guide to the eye (see text). Right: Rényi entanglement entropy as a function of $1/q$ as obtained from our QMC calculation compared to the DMRG result. The horizontal line corresponds to S_{∞}^E obtained from DMRG. We also show the lowest energy level of the reconstructed entanglement spectrum from the QMC data as a function of $1/q_{\max}$ and the function $\frac{q-1}{q} S_q^E$ from the QMC result. Remarkably, both curves tend to S_{∞}^E equally fast, however obtaining S_{∞}^E from the large q limit of $\frac{q-1}{q} S_q^E$ may be more reliable.

tanglement spectrum using $q_{\max} = 4$. Here, we perform a similar calculation for the entanglement spectrum of a $L = 10$ Heisenberg ladder (see Fig. 7, using the same bipartition as previously) for $J_{\perp} = J$ and focus on the role of systematic and statistical errors. As in Ref. 19, we split the reduced density matrix in its symmetry sectors and perform the calculation in each sector (see Appendix B).

We have calculated the Rényi entanglement entropies up to $q_{\max} = 9$ with the QMC method described above for the sectors $S_z = 0, 1$ and 2 (q_{\max} decreases with S_z due to too large entropies) and reconstructed the entanglement spectrum, systematically varying q_{\max} in order to demonstrate the rate of convergence towards the exact entanglement spectrum obtained from DMRG. In Fig. 9, we also show the reconstructed spectrum from the exact DMRG entanglement entropies. The deviation of the reconstructed DMRG spectrum from the exact spectrum gives an impression of the systematic error due to the truncation of the polynomial, while the reconstructed QMC spectrum carries additional errors due to the statistical uncertainty of the entanglement entropies.

The convergence of the lowest level (largest eigenvalue λ_0 of ρ_A) in the sector $S_z = 0$ is very good and the QMC result is trustworthy. This result corresponds to the single copy entanglement entropy $S_{A,\infty}^E = -\ln \lambda_0$ for which no direct QMC estimate is available. The lowest level in the sector $S_z = 1$ also seems to be converged (within errorbars), however, judging from the QMC data only, it is

not possible to decide whether the result is trustworthy or not. All other levels can not be trusted due to the statistical uncertainty. Therefore, one should bear in mind that a careful convergence analysis with q_{\max} has to be carried out and that in general only the lowest part of the entanglement spectrum can be extracted from QMC data bearing statistical uncertainties. The reconstructed spectrum from the exact DMRG entanglement entropies shows in particular, how slowly higher levels of the entanglement spectrum converge with q_{\max} . This is the reason why it is beneficial to split the calculation in symmetry sectors.

A global view on the full entanglement spectrum, resolved in spin sectors, is provided in Fig. 10 (left) where the exact entanglement levels from DMRG are compared to the reconstruction from QMC data. A parabolic envelope is shown, as expected from the low energy spectrum of XXZ chains⁴⁷. The right panel of Fig. 10 shows that besides the reconstruction method, it is also possible to accept the single copy entanglement $S_{A,\infty}^E$ using an extrapolation in $q/(q-1)$ of the Rényi entanglement entropies $S_{A,q}^E$.

D. Entanglement Hamiltonian

Given the difficulty of the extraction of the entanglement spectrum from QMC data, different methods of the verification of effective entanglement Hamiltonians and the extraction of the inverse entanglement temperature β_{eff} should be explored. We have proposed the usage of the participation spectrum for this purpose in a previous work²⁸, which can only provide partial proof that the effective model is correct. Here, we propose a different and in fact complementary method that relies on the comparison of the Rényi entanglement entropy and the finite temperature thermodynamic Rényi entropy of a putative entanglement Hamiltonian.

The reduced density matrix ρ_A can be expressed as a thermal mixed state of an effective entanglement Hamiltonian \hat{H}_E at inverse temperature β_{eff} by

$$\rho_A = \frac{1}{Z} e^{-\beta_{\text{eff}} \hat{H}_E}, \quad (28)$$

with $Z = \text{Tr} e^{-\beta_{\text{eff}} \hat{H}_E}$. Therefore, the thermodynamic entropies S_q^{th} of the effective model \hat{H}_E at inverse temperature β_{eff} have to be equal to the entanglement entropies $S_{A,q}^E$ for all q , which is obvious from the above definition Eq. (28) of \hat{H}_E .

In the case of the strongly entangled Heisenberg ladder ($J_{\perp} > J$), it was shown within first order perturbation theory^{40,41,43,45} that the entanglement Hamiltonian is given by the simple Heisenberg chain at an effective inverse temperature of $2/J_{\perp}$. The second order correction for the effective temperature (*cf.* Eq. (21) in Ref. 43,

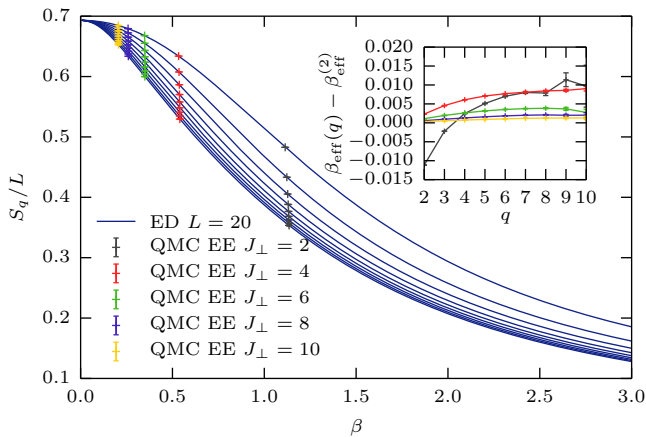


Figure 11: (Color online) Comparison of the thermodynamic Rényi entropy of the XXX chain for $q = 2$ (top curve) to $q = 10$ (bottom curve) and the entanglement Rényi entropy of the Heisenberg ladder using several values of J_{\perp}/J (coloured symbols). For every value of q , we calculate the inverse temperature β at which the entanglement entropy matches the thermodynamic entropy of the XXX chain. The inset displays the deviation of the corresponding effective inverse temperatures β_{eff} from the second order result $\beta_{\text{eff}}^{(2)} = \frac{2}{J_{\perp}} + \frac{1}{2J_{\perp}^2}$ (cf. Ref. 43) as a function of q (see main text).

ignoring next nearest neighbor interactions) yields

$$\beta_{\text{eff}}^{(2)} = \frac{2}{J_{\perp}} + \frac{1}{2J_{\perp}^2}. \quad (29)$$

In Figure 11, we explore the regime of validity of the first-order entanglement Hamiltonian. We display $S_q^{\text{th}}(\beta)$ of the $L = 20$ Heisenberg chain for different Rényi indices q as a function of inverse temperature β . Then, we calculate the entanglement entropy of the $L = 20$ Heisenberg ladder for different values of $J_{\perp} = 2, 4, 6, 8, 10$ with our QMC method and extract the effective inverse temperature for which the two quantities match. If the entanglement Hamiltonian is correct, the resulting effective inverse temperature has to be independent of q . This is clearly the case if J_{\perp}/J becomes large, as visible both in main panel and inset of Fig. 11, where the deviation from Eq. 29 is getting smaller and flatter (as a function of q) when J_{\perp} increases.

VI. CONCLUSION

We have shown that the calculation of entanglement Rényi entropies may be split into two independent Monte Carlo simulations, one of which boils down to a standard calculation of the participation Rényi entropy S_q^{PR} obtained from a simulation of q independent replicas, while the other part is a “replica correlation” entropy C_q^{R} obtained in a simulation of q replicas glued together on subsystem A . As the PR entropy is a basis dependent

quantity, C_q^{R} has to be basis dependent, too. Both quantities have to be calculated in the same basis to obtain the correct entanglement entropy.

In a second step, we have developed an improved estimator for the PR entropy, exploiting the fact that the independent replicas can be transformed independently under imaginary time and space symmetry transformations leaving the weight of the Monte Carlo configuration invariant. The number of configurations that are averaged over is therefore multiplied by a number growing exponentially with the number of replicas q and counteracts the exponential decay of the probability of finding identical states in all replicas with q . This improved estimator allows us to measure extremely low probabilities, crucial for the calculations of S_q^E for large values of the Rényi index q .

Given that the two terms S_q^{PR} and C_q^{R} exhibit a volume law, the realm of applicability of the method is limited to cases, where C_q^{R} is not too large. This is precisely the case in situations where the circumference of subsystem A is identical to its volume such as for the example of the ladders studied in this article. Here, the largest contribution to the entanglement entropy stems from the PR entropy, which can be calculated with very good precision due to the improved estimator.

For situations where the volume of the subsystem becomes large, such as the half system of a two dimensional lattice, it is possible to combine the two methods to calculate the entanglement entropy. This would result for example to perform the first increment (*i.e.* a line-shaped subsystem) with the method presented here with very good precision and start from there exploiting a ratio trick^{14,29} using the method introduced in Ref. 16. This way, the largest growth of entanglement entropy is dealt with by the improved estimator and the addition of further lattice sites to the subsystem does not increase the entanglement dramatically, therefore the ratio trick method is supposed to work very well without accumulating larger errors.

Let us finally note that the lessons from the improved estimator can certainly be implemented in the method introduced by Humeniuk and Roscilde¹⁶. If the QMC configuration is in the independent ensemble, one can check if any of the symmetry transformed replica configurations introduced here matches the gluing condition. If so, one has to actually perform the transformation of the whole operator string: in practice, this may turn computationally expensive and one would need to check in which situations the improvement in statistics will be worth the additional computational extra-cost.

VII. ACKNOWLEDGEMENTS

We wish to thank S. Capponi for discussions and for providing test data, D. Poilblanc, S. Pujari and S. Wesel for useful related discussions and I. McCulloch for providing access to his code⁵² used to perform the test

DMRG calculations. Our QMC codes are partly based on the ALPS libraries^{48,49}. This work was performed using HPC resources from GENCI (grant x2014050225) and CALMIP (grant 2014-P0677) and is supported by the French ANR program ANR-11-IS04-005-01. We also acknowledge the technical assistance by the IDRIS supercomputer center.

Appendix A: Improved estimator of thermal Rényi entropies

In order to be explicit, let us start from Eq. (19) and concentrate on the ratio of partition functions that have

$$\frac{Z(q\beta)}{Z(\beta)^q} = \frac{\sum_{\alpha} \sum_{S_{\Lambda}} (-1)^{n_2} \frac{(q\beta)^n (\Lambda-n)!}{\Lambda!} \langle \alpha | \prod_{p=0}^{\Lambda-1} H_{a(p),b(p)} | \alpha \rangle}{\sum_{\alpha_1 \dots \alpha_q} \sum_{S_{\Lambda}^1 \dots S_{\Lambda}^q} (-1)^{n_2} \frac{\beta^n \prod_{i=1}^q (\Lambda_i - n_i)!}{\prod_{i=1}^q \Lambda_i!} \prod_{i=1}^q \langle \alpha_i | \prod_{p=0}^{\Lambda_i-1} H_{a_i(p),b_i(p)} | \alpha_i \rangle}. \quad (\text{A1})$$

Let us now introduce the observable to compute the PR entropy S_q^{PR} in the ensemble of q independent repli-

cas. It is given by the Kronecker delta $\delta_{\alpha_1, \dots, \alpha_q}$.

$$\begin{aligned} \frac{Z(q\beta)}{Z(\beta)^q} &= \frac{\sum_{\alpha} \sum_{S_{\Lambda}^1 \dots S_{\Lambda}^q} (-1)^{n_2} \frac{\beta^n \prod_{i=1}^q (\Lambda_i - n_i)!}{\prod_{i=1}^q \Lambda_i!} \prod_{i=1}^q \langle \alpha | \prod_{p=0}^{\Lambda_i-1} H_{a_i(p),b_i(p)} | \alpha \rangle}{\sum_{\alpha_1 \dots \alpha_q} \sum_{S_{\Lambda}^1 \dots S_{\Lambda}^q} (-1)^{n_2} \frac{\beta^n \prod_{i=1}^q (\Lambda_i - n_i)!}{\prod_{i=1}^q \Lambda_i!} \prod_{i=1}^q \langle \alpha_i | \prod_{p=0}^{\Lambda_i-1} H_{a_i(p),b_i(p)} | \alpha_i \rangle} \times \\ &\times \frac{\sum_{\alpha} \sum_{S_{\Lambda}} (-1)^{n_2} \frac{(q\beta)^n (\Lambda-n)!}{\Lambda!} \langle \alpha | \prod_{p=0}^{\Lambda-1} H_{a(p),b(p)} | \alpha \rangle}{\sum_{\alpha} \sum_{S_{\Lambda}^1 \dots S_{\Lambda}^q} (-1)^{n_2} \frac{\beta^n \prod_{i=1}^q (\Lambda_i - n_i)!}{\prod_{i=1}^q \Lambda_i!} \prod_{i=1}^q \langle \alpha | \prod_{p=0}^{\Lambda_i-1} H_{a_i(p),b_i(p)} | \alpha \rangle} = \\ &e^{(1-q)S_q^{\text{PR}}} \times \frac{\sum_{\alpha} \sum_{S_{\Lambda}} (-1)^{n_2} \frac{(q\beta)^n (\Lambda-n)!}{\Lambda!} \langle \alpha | \prod_{p=0}^{\Lambda-1} H_{a(p),b(p)} | \alpha \rangle}{\sum_{\alpha} \sum_{S_{\Lambda}(\Lambda_1, \dots, \Lambda_q)} \delta_{\alpha_1, \Lambda_1, \dots, \alpha_q, \Lambda_q} \frac{\Lambda! \prod_{i=1}^q (\Lambda_i - n_i)!}{q^n (\Lambda-n)! \prod_{i=1}^q \Lambda_i!} (-1)^{n_2} \frac{(q\beta)^n (\Lambda-n)!}{\Lambda!} \langle \alpha | \prod_{p=0}^{\Lambda-1} H_{a(p),b(p)} | \alpha \rangle}, \end{aligned} \quad (\text{A2})$$

where in the last step, we reexpressed the q independent replicas in terms of a unique system at inverse temperature $q\beta$. This is done by introducing a partition $(\Lambda_1, \dots, \Lambda_q)$ of the operator string S_{Λ} into q parts such that the cutoffs sum up to Λ : $\sum_i \Lambda_i = \Lambda$. Clearly, in all the expressions above, the numbers of (offdiagonal) operators n_i ($n_2^{(i)}$) in slice i of the operator string also have to sum up to the complete number of (offdiagonal) operators n (n_2). The introduction of the Kronecker delta $\delta_{\alpha_1, \Lambda_1, \dots, \alpha_q, \Lambda_q}$ expresses the fact that only operator strings in which the states $|\alpha_i, \Lambda_i\rangle$ at the end of each slice i are identical will contribute to our result.

Alltogether, we see that we have to perform an SSE calculation at inverse temperature $q\beta$ and measure the observable:

$$\delta_{\alpha_1, \Lambda_1, \dots, \alpha_q, \Lambda_q} \frac{\Lambda! \prod_{i=1}^q (\Lambda_i - n_i)!}{q^n (\Lambda-n)! \prod_{i=1}^q \Lambda_i!}. \quad (\text{A3})$$

Appendix B: Rényi entanglement entropies by S_z sector

Here, we provide some additional details on the reconstruction of the entanglement spectrum by symmetry sectors (here S_z sectors) of the reduced density matrix using the method described in Refs. 19,31. Since the reduced density matrix ρ_A is block-diagonal with S_z of subsystem A , we can split the calculation into the blocks $\rho_A^{S_z}$.

The first observation is that the normalization of each block is no longer given by 1, but by the probability p_{S_z} of finding a state with subsystem magnetization equal to S_z :

$$\text{Tr} \rho_A^{S_z} = p_{S_z}, \quad (\text{B1})$$

which is easily measured in the independent ensemble. This is of course the first power sum of the eigenvalues of $\rho_A^{S_z}$.

We can calculate the q -th power sum of $\rho_A^{S_z}$ by using the same method as described in the main text by just ignoring in the measurement states that are not in the correct sector. However, this would corresponds to a reduced density matrix $\tilde{\rho}_A$ which is normalized to 1. In order to obtain the correct normalization, we calculate

$$\text{Tr} \left(\rho_A^{S_z} \right)^q = p_{S_z}^q \frac{p_{\emptyset \rightarrow A}(S_z)}{p_{A \rightarrow \emptyset}(S_z)}, \quad (\text{B2})$$

where $p_{\emptyset \rightarrow A}(S_z)$ and $p_{A \rightarrow \emptyset}(S_z)$ correspond to the transition probabilities estimated from measurements in the corresponding S_z sector only. Note that these probabilities can be obtained by binning the measurements of the transition probabilities by their S_z sectors *without changing their normalization* and then by dividing by the probability of being in the correct sector in the corresponding ensemble (for the independent ensemble, this cancels exactly the factor $p_{S_z}^q$).

From the knowledge of the power sums of the eigenvalues of $\rho_A^{S_z}$ we can now use the method described by Song *et al.*³¹ to reconstruct the entanglement spectrum. Note however, that in equation (2.30) of Ref. 31 the 1 on the diagonal has to be replaced by the first power sum of the eigenvalues of $\rho_A^{S_z}$, *i.e.* by $p_{S_z} = \text{Tr} \rho_A^{S_z}$.

* Electronic address: luitz@irsamc.ups-tlse.fr

- ¹ A. Einstein, B. Podolsky, and N. Rosen, Phys. Rev. **47**, 777 (1935), URL <http://link.aps.org/doi/10.1103/PhysRev.47.777>.
- ² P. Calabrese, J. Cardy, and B. Doyon, Journal of Physics A: Mathematical and Theoretical **42**, 500301 (2009), URL <http://stacks.iop.org/1751-8121/42/i=50/a=500301>.
- ³ B.-Q. Jin and V. Korepin, Journal of Statistical Physics **116**, 79 (2004), ISSN 0022-4715, URL <http://dx.doi.org/10.1023/B%3AJOSS.0000037230.37166.42>.
- ⁴ H. Fan, V. Korepin, and V. Roychowdhury, Phys. Rev. Lett. **93**, 227203 (2004), URL <http://link.aps.org/doi/10.1103/PhysRevLett.93.227203>.
- ⁵ P. Calabrese and J. Cardy, J. Stat. Mech. **2004**, P06002 (2004), ISSN 1742-5468, URL <http://iopscience.iop.org/1742-5468/2004/06/P06002>.
- ⁶ G. Refael and J. E. Moore, Phys. Rev. Lett. **93**, 260602 (2004), URL <http://link.aps.org/doi/10.1103/PhysRevLett.93.260602>.
- ⁷ U. Schollwöck, Rev. Mod. Phys. **77**, 259 (2005), URL <http://link.aps.org/doi/10.1103/RevModPhys.77.259>.
- ⁸ A. B. Kallin, M. B. Hastings, R. G. Melko, and R. R. P. Singh, Phys. Rev. B **84**, 165134 (2011), URL <http://link.aps.org/doi/10.1103/PhysRevB.84.165134>.
- ⁹ R. R. P. Singh, R. G. Melko, and J. Oitmaa, Phys. Rev. B **86**, 075106 (2012), URL <http://link.aps.org/doi/10.1103/PhysRevB.86.075106>.
- ¹⁰ A. B. Kallin, K. Hyatt, R. R. P. Singh, and R. G. Melko, Phys. Rev. Lett. **110**, 135702 (2013), URL <http://link.aps.org/doi/10.1103/PhysRevLett.110.135702>.
- ¹¹ A. B. Kallin, E. M. Stoudenmire, P. Fendley, R. R. P. Singh, and R. G. Melko, arXiv e-print 1401.3504 (2014), URL <http://arxiv.org/abs/1401.3504>.
- ¹² F. Alet, S. Capponi, N. Laflorencie, and M. Mambrini, Phys. Rev. Lett. **99**, 117204 (2007), URL <http://link.aps.org/doi/10.1103/PhysRevLett.99.117204>.
- ¹³ A. B. Kallin, I. González, M. B. Hastings, and R. G. Melko, Phys. Rev. Lett. **103**, 117203 (2009), URL <http://link.aps.org/doi/10.1103/PhysRevLett.103.117203>.
- ¹⁴ M. B. Hastings, I. González, A. B. Kallin, and R. G. Melko, Phys. Rev. Lett. **104**, 157201 (2010), URL <http://link.aps.org/doi/10.1103/PhysRevLett.104.157201>.
- ¹⁵ R. G. Melko, A. B. Kallin, and M. B. Hastings, Phys. Rev. B **82**, 100409 (2010), URL <http://link.aps.org/doi/10.1103/PhysRevB.82.100409>.
- ¹⁶ S. Humeniuk and T. Roscilde, Phys. Rev. B **86**, 235116 (2012), URL <http://link.aps.org/doi/10.1103/PhysRevB.86.235116>.
- ¹⁷ T. Grover, Phys. Rev. Lett. **111**, 130402 (2013), URL <http://link.aps.org/doi/10.1103/PhysRevLett.111.130402>.
- ¹⁸ F. F. Assaad, T. C. Lang, and F. Parisen Toldin, Phys. Rev. B **89**, 125121 (2014), URL <http://link.aps.org/doi/10.1103/PhysRevB.89.125121>.
- ¹⁹ C.-M. Chung, L. Bonnes, P. Chen, and A. M. Läuchli, arXiv:1305.6536 [cond-mat] (2013), URL <http://arxiv.org/abs/1305.6536>.
- ²⁰ J. Helmes and S. Wessel, ArXiv e-prints (2014), 1403.7395.
- ²¹ C. M. Herdman, P.-N. Roy, R. G. Melko, and A. Del Maestro, Phys. Rev. B **89**, 140501 (2014), URL <http://link.aps.org/doi/10.1103/PhysRevB.89.140501>.
- ²² A. W. Sandvik, AIP Conference Proceedings **1297**, 135 (2010), ISSN 0094243X, URL http://proceedings.aip.org/resource/2/apcpcs/1297/1/135_1.
- ²³ M.-C. Chung and I. Peschel, Phys. Rev. B **64**, 064412 (2001), URL <http://link.aps.org/doi/10.1103/PhysRevB.64.064412>.
- ²⁴ K. Audenaert, J. Eisert, M. B. Plenio, and R. F. Werner, Phys. Rev. A **66**, 042327 (2002), URL <http://link.aps.org/doi/10.1103/PhysRevA.66.042327>.
- ²⁵ S. Inglis and R. G. Melko, Phys. Rev. E **87**, 013306 (2013), URL <http://link.aps.org/doi/10.1103/PhysRevE.87.013306>.
- ²⁶ D. J. Luitz, F. Alet, and N. Laflorencie, Phys. Rev. Lett. **112**, 057203 (2014), URL <http://link.aps.org/doi/10.1103/PhysRevLett.112.057203>.

- ²⁷ D. J. Luitz, F. Alet, and N. Laflorencie, Phys. Rev. B **89**, 165106 (2014), URL <http://link.aps.org/doi/10.1103/PhysRevB.89.165106>.
- ²⁸ D. J. Luitz, N. Laflorencie, and F. Alet, arXiv e-print 1403.3717 (2014), URL <http://arxiv.org/abs/1404.3713>.
- ²⁹ P. de Forcrand, M. D'Elia, and M. Pepe, Phys. Rev. Lett. **86**, 1438 (2001), URL <http://link.aps.org/doi/10.1103/PhysRevLett.86.1438>.
- ³⁰ J.-M. Stéphan, S. Furukawa, G. Misguich, and V. Pasquier, Physical Review B **80**, 184421 (2009), ISSN 1098-0121, 1550-235X, URL <http://link.aps.org/doi/10.1103/PhysRevB.80.184421>.
- ³¹ H. F. Song, S. Rachel, C. Flindt, I. Klich, N. Laflorencie, and K. Le Hur, Phys. Rev. B **85**, 035409 (2012), URL <http://link.aps.org/doi/10.1103/PhysRevB.85.035409>.
- ³² J.-M. Stéphan, G. Misguich, and V. Pasquier, Physical Review B **82**, 125455 (2010), ISSN 1098-0121, 1550-235X, URL <http://link.aps.org/doi/10.1103/PhysRevB.82.125455>.
- ³³ J.-M. Stéphan, G. Misguich, and V. Pasquier, Physical Review B **84**, 195128 (2011), ISSN 1098-0121, 1550-235X, URL <http://link.aps.org/doi/10.1103/PhysRevB.84.195128>.
- ³⁴ J. Eisert, M. Cramer, and M. B. Plenio, Reviews of Modern Physics **82**, 277 (2010), URL <http://link.aps.org/doi/10.1103/RevModPhys.82.277>.
- ³⁵ W. Kahan, Commun. ACM **8**, 40 (1965), ISSN 0001-0782, URL <http://doi.acm.org/10.1145/363707.363723>.
- ³⁶ P. Calabrese, M. Campostrini, F. Essler, and B. Nienhuis, Phys. Rev. Lett. **104**, 095701 (2010), URL <http://link.aps.org/doi/10.1103/PhysRevLett.104.095701>.
- ³⁷ J. L. Cardy, Journal of Physics A: Mathematical and General **19**, L1093 (1986), URL <http://stacks.iop.org/0305-4470/19/i=17/a=008>.
- ³⁸ I. Affleck, Phys. Rev. Lett. **56**, 746 (1986), URL <http://link.aps.org/doi/10.1103/PhysRevLett.56.746>.
- ³⁹ D. Poilblanc, Phys. Rev. Lett. **105**, 077202 (2010), URL <http://link.aps.org/doi/10.1103/PhysRevLett.105.077202>.
- ⁴⁰ A. M. Läuchli and J. Schliemann, Phys. Rev. B **85**, 054403 (2012), URL <http://link.aps.org/doi/10.1103/PhysRevB.85.054403>.
- ⁴¹ I. Peschel and M.-C. Chung, EPL (Europhysics Letters) **96**, 50006 (2011), URL <http://stacks.iop.org/0295-5075/96/i=5/a=50006>.
- ⁴² J. I. Cirac, D. Poilblanc, N. Schuch, and F. Verstraete, Phys. Rev. B **83**, 245134 (2011), URL <http://link.aps.org/doi/10.1103/PhysRevB.83.245134>.
- ⁴³ J. Schliemann and A. M. Läuchli, J. Stat. Mech. **2012**, P11021 (2012), ISSN 1742-5468, URL <http://iopscience.iop.org/1742-5468/2012/11/P11021>.
- ⁴⁴ R. Lundgren, V. Chua, and G. A. Fiete, Phys. Rev. B **86**, 224422 (2012), URL <http://link.aps.org/doi/10.1103/PhysRevB.86.224422>.
- ⁴⁵ X. Chen and E. Fradkin, Journal of Statistical Mechanics: Theory and Experiment **2013**, P08013 (2013), URL <http://stacks.iop.org/1742-5468/2013/i=08/a=P08013>.
- ⁴⁶ R. Lundgren, Y. Fuji, S. Furukawa, and M. Oshikawa, Phys. Rev. B **88**, 245137 (2013), URL <http://link.aps.org/doi/10.1103/PhysRevB.88.245137>.
- ⁴⁷ F. C. Alcaraz, M. N. Barber, and M. T. Batchelor, Phys. Rev. Lett. **58**, 771 (1987), URL <http://link.aps.org/doi/10.1103/PhysRevLett.58.771>.
- ⁴⁸ A. Albuquerque, F. Alet, P. Corboz, P. Dayal, A. Feiguin, S. Fuchs, L. Gamper, E. Gull, S. Grtler, A. Honecker, et al., Journal of Magnetism and Magnetic Materials **310**, 1187 (2007), ISSN 0304-8853, URL <http://www.sciencedirect.com/science/article/pii/S0304885306014983>.
- ⁴⁹ B. Bauer, L. D. Carr, H. G. Evertz, A. Feiguin, J. Freire, S. Fuchs, L. Gamper, J. Gukelberger, E. Gull, S. Guertler, et al., Journal of Statistical Mechanics: Theory and Experiment **2011**, P05001 (2011), URL <http://stacks.iop.org/1742-5468/2011/i=05/a=P05001>.
- ⁵⁰ It should be noted that this problem only occurs in the regime of very large PR entropies, far beyond the reach of the simple estimator given in Eq. (12).
- ⁵¹ The use of open chains simplifies the problem of computing thermal averages in the free fermion representation of the XX spin- $\frac{1}{2}$ chain.
- ⁵² See <http://physics.uq.edu.au/people/ianmcc/mptoolkit/>